Journal of Alloys and Compounds 525 (2012) 68–72

Contents lists available at SciVerse ScienceDirect

Journal of Alloys and Compounds

journal homepage: www.elsevier.com/locate/jallcom

Plasticity enhancement of Zr-based bulk metallic glasses by direct current electropulsing

P. Yiu [a], J.S.C. Jang [b], S.Y. Chang [c], Y.C. Chen [d], J.P. Chu [d], C.H. Hsueh [a,*]

[a] Department of Materials Science and Engineering, National Taiwan University, Taipei 10617, Taiwan
[b] Institute of Materials Science and Engineering, National Central University, Jhongli 32001, Taiwan
[c] Department of Materials Science and Engineering, National Chung Hsing University, Taichung 402, Taiwan
[d] Department of Materials Science and Engineering, National Taiwan University of Science & Technology, Taipei 10607, Taiwan

ARTICLE INFO

Article history:
Received 28 December 2011
Received in revised form 7 February 2012
Accepted 9 February 2012
Available online xxx

Keywords:
Metallic glasses
Amorphous materials
Mechanical properties
Nanoindentation
Shear band
Electropulsing

ABSTRACT

Direct current electropulsing was used to improve the plasticity of $(Zr_{53}Cu_{30}Ni_9Al_8)_{99.5}Si_{0.5}$ bulk metallic glasses. After the electropulsing treatment, the specimen showed reductions in both the glass transition and the crystallization temperatures while retaining its amorphous structure, and both Young's modulus and the hardness decreased while the nanoindentation loading curve became more serrated. Using the bond-interface method and Vickers indentation, the treated specimen showed more branching of semi-circular shear bands and less radial shear bands compared to its as-cast counterpart. The possible plasticity enhancement mechanism of the electropulsing treatment was also discussed.

1. Introduction

Bulk metallic glasses (BMGs) are alloys quenched from the melt at a cooling rate high enough to suppress nucleation and growth of crystalline phases. The resulting solid amorphous material shows no crystalline structure and, hence, no dislocations and grain boundaries. For this reason, BMGs constitute a new class of metallic materials with attractive mechanical properties, including near theoretical strength, high hardness, extremely low damping characteristics, excellent wear properties, and good potential for forming and shaping in the supercooled region [1,2]. However, because of the amorphous structure, our traditional understanding of the behavior of crystalline metals governed by dislocation plasticity does not apply, and the deformation behavior of BMGs is not well understood at the present time even after extensive studies. Nevertheless, BMGs often deform by the formation of localized shear bands and display little plasticity before catastrophic fracture at room temperature [1–3]. In the past decade, efforts have been devoted to improve the plasticity of BMGs, and various methods like reinforcing inclusions [4–8] and in situ formation of second phases [9–11] have been developed. Other than making BMGs into a composite, plasticity can also be enhanced by shot peening, introducing porosity, pre-compression, and controlling of the solidification condition [12–15].

Electropulsing treatment (EPT) has been developed since the late eighties as a competitive technique to traditional annealing on the microstructural control and mechanical property modification of engineering alloys such as Mg–Al–Zn, Zn–Al and Fe–Si etc. [16–20]. It has also been applied on BMGs for accelerated crystallization [21,22] and welding [23]. However, the influence of high current density electric pulses on the mechanical properties of BMGs was rarely discussed. Recently, it was reported that EPT could enhance the compressive ductility of $Zr_{62}Al_{19}Ni_{19}$ BMG by more than 5% while keeping the alloy amorphous [24]. However, the mechanism for the modification of shear band behavior by EPT was left unanswered. In the present work, nanoindentation was performed on electropulsing-treated Zr-based BMGs to investigate the possible plasticity enhancement mechanism of EPT.

2. Experimental procedures

An alloy ingot with composition of $(Zr_{53}Cu_{30}Ni_9Al_8)_{99.5}Si_{0.5}$ by at% was prepared by arc melting the mixture of corresponding pure elements, Zr (99.8 wt% purity), Ni (99.9 wt% purity), Cu (99.99 wt% purity), Al (99.99 wt% purity), and Si (99.99% purity), in a Ti-gettered argon atmosphere. Then, the alloy ingot was remelted in the same atmosphere prior to casting. Finally the ingot was melted again and the liquid alloy was drop casted into a water-cooled copper mold to form an alloy rod

* Corresponding author. Tel.: +886 2 33661307; fax: +886 2 23634562.
E-mail address: hsuehc@ntu.edu.tw (C.H. Hsueh).

0925-8388/$ – see front matter © 2012 Elsevier B.V. All rights reserved.
doi:10.1016/j.jallcom.2012.02.074

of 3 mm in diameter. The rod was then cut into rectangular beams of dimensions 2 mm × 1 mm × 20 mm each.

In the present study, electropulsing was generated by a pulsed direct current (DC) power supply with square waves of duration 0.1 ms per pulse at a frequency of 15 Hz. The peak output was 30 V/0.8 A resulting in a current density of 40 A/cm^2. A pair of high purity copper block was used to fix the two ends of the BMG beam. Separation between copper blocks, which also served as electrodes, was 10 mm. EPT was performed at room temperature, and post-treatment cooling was done in still air. Differential scanning calorimetry (DSC) was done with Seiko Instrument DSC6200 at a heating rate of 40 K/min in Nitrogen atmosphere. Electron diffraction pattern and imaging were performed in Tecnai G^2 F20 200 kV TEM. Nanoindentations were carried out with Hysitron TriboLab Nanoindenter at different loading rates (0.1, 0.2, 0.4, and 1.6 mN/s) without holding at the peak load. The average thermal drift was below 0.5 nm/s. Finally, a bond-interface method was applied to observe the shear band pattern underneath a Vickers indentation. In this method, a BMG beam was cut into two halves. The flat cutting surface of each half was ground and mirror polished with 1 μm alumina powders and the two mirror surfaces were then glued face to face. Vickers indentations of 1 kgf were performed over the top of the interface with the indent mark located right in the middle. The glued compound was then separated back into halves with a warm acetone bath for 24 h, and the vertical cross-section of Vickers indentation was revealed. SEM images of the cross-section were taken using a FEI Quanta 3D FEG.

3. Results and discussion

DSC and selected area electron diffraction were used to characterize the crystallinity of the as-cast and the EPT $(Zr_{53}Cu_{30}Ni_9Al_8)Si_{0.5}$ BMGs. The glass transition temperature and the crystallization temperature of the as-cast BMG were 754 K and 790 K, respectively, whereas those of the EPT BMG were reduced to 750 K and 774 K, respectively. Both curves showed a step at glass transition as well as a one-step crystallization peak, implying that the crystallization kinetics was unchanged after EPT. High resolution TEM micrographs and diffraction patterns of the as-cast and the EPT BMGs are showed, respectively, in Fig. 1(a) and (b). No crystalline phase can be observed in the micrographs and typical diffused rings are shown in the diffraction patterns, implying an amorphous structure for both the as-cast and the EPT BMGs. This result agreed with Zhang and Shek's result [24] that EPT only caused peak-shift in DSC while the specimen remained amorphous.

The measured Young's modulus and hardness of BMGs before and after EPT are listed in Table 1. The modulus and hardness of the EPT BMG are always lower than those of the as-cast BMG. It was suggested that the extent for the BMG to deform plastically could be characterized by the following plastic criterion [25]:

$$R_w = \frac{W_p}{W_t} = \frac{h_f}{h_{\max}} \quad (1)$$

where W_p and W_t are the work done by plastic deformation and total deformation, and h_f and $h_{\max}$ are the residual displacement after unloading and the displacement at the maximum load, respectively. The calculated R_w is also summarized in Table 1. The slight increase of R_w after EPT indicates that EPT BMG is more prone to plastic deformation. The comparison of complete indentation load–displacement (P–h) curves between the as-cast and the EPT BMGs at an indentation rate of 0.1 mN/s is shown in Fig. 2. Serrations are present in both curves; however, there are more serrations for the EPT BMG. As pop-in events signify discrete plasticity; i.e., shear band propagation [26], this is believed to be the evidence of improved plasticity.

The loading portions of the P–h curves at different loading rates are shown in Fig. 3(a) and (b), respectively, for the as-cast and the EPT BMGs. The curves are offset from zero displacement for clarity. Compared to Fig. 3(a) and (b) shows more serrations for all loading rates and the serration starts at an earlier stage upon loading. It should be noted that the curves in both Fig. 3(a) and (b) become smoother as the loading rate increases. This signifies a transition from inhomogeneous to homogeneous plastic deformation with the increasing loading rate as suggested by Schuh et al.

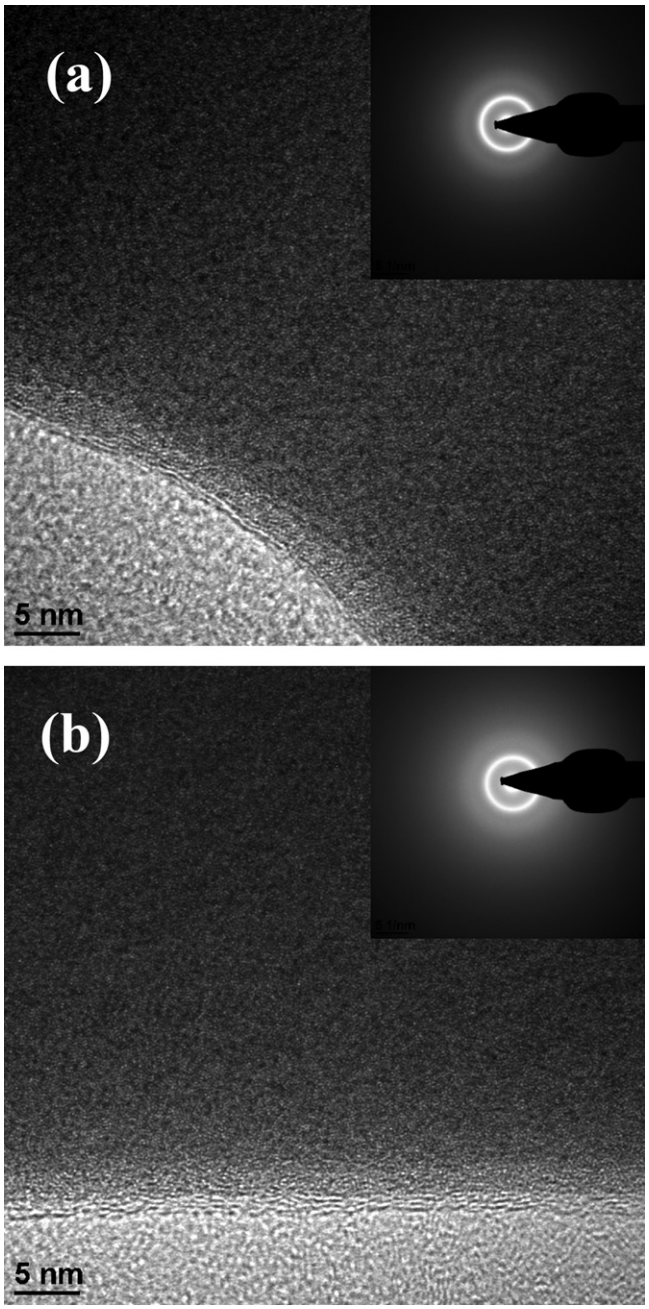

Fig. 1. High resolution TEM micrograph and electron diffraction pattern (inset) showing the amorphous structure of (a) as-cast and (b) EPT BMGs.

[26]. It was concluded that homogeneity under high loading rates was due to shear transformation zones (STZs) clustered and moved collectively upon deformation. As STZs acted as embryos of shear bands, shear bands would have fewer sites to nucleate upon deformation if they responded to deformation in terms of cluster [27]. In the present work, serration steps still can be clearly observed at loading rate as high as 1.6 mN/s for the EPT BMG while they become almost indistinguishable for the as-cast BMG. Therefore, more serrations in the loading curve for the EPT BMG signify more likely to deform with discrete plasticity; i.e., forming more shear bands upon deformation. In contrast, serrations in the P–h curves of annealing embrittled BMGs are always flattened because of the annihilation of free volume by the structural relaxation regardless whether crystallization occurs after annealing [28–30].

Table 1
Mechanical properties of as-cast and EPT BMGs measured using nanoindentation.

Sample	Loading rate (mN/s)	Modulus E (GPa)	Hardness H (GPa)	Plastic criterion R_w
As-cast BMG	0.1	101.15	11.29	0.434
	0.2	114.51	9.02	0.573
	0.4	120.06	8.25	0.617
	1.6	125.29	7.97	0.629
EPT	0.1	88.62	10.31	0.446
BMG	0.2	92.61	7.27	0.582
	0.4	103.95	6.72	0.652
	1.6	102.30	7.13	0.631

Using the bond-interface method, the micrographs of subsurface shear band patterns induced by Vickers indentation on the as-cast and the EPT BMGs are shown in Fig. 4(a) and (b), respectively. The typical shear band pattern; i.e., semi-circular (referred as primary) and radial (referred as secondary) shear bands, can be observed in Fig. 4(a). However, a fractured region underneath the indenter tip and severe cracking along primary shear bands as indicated by arrows in Fig. 4(a) are also observed for the as-cast BMG. In the meanwhile, the radial shear bands are less obvious in Fig. 4(b) for the EPT BMG. Instead, the tails of semi-circular shear bands are more branched than the as-cast BMG, as indicated by arrows. Higher magnification images of the selected area (marked by rectangle) in Fig. 4(a) and (b) are shown in Fig. 5(a) and (b). The angle formed at the intersection of a pair of secondary shear band shown in Fig. 5(a) is about 90°, while there exists abundant branching between semi-circular shear bands in Fig. 5(b). Indentation studies of BMGs showed that primary shear bands were formed first as a response to the compressive stress until saturation and secondary shear bands were then formed and kinked the primary shear bands [31]. It can be seen that the secondary shear bands are less obvious and the kinks of primary shear bands are smaller in the EPT BMG than the as-cast BMG.

Based on the expanding cavity model, it has been shown that the plastic flow underneath the indenter is dominated by the compression mechanism which results in the formation of semi-circular shear bands [32,33]. Also, using the bond-interface method and Vickers indentation, shear band patterns have been studied for various BMGs. While the patterns reveal more semi-circular shear bands for highly ductile Pd-based BMGs, [34,35], radial shear bands are more prone to form for less-ductile Zr- or Fe-based BMGs [32,33]. Hence, it can be concluded that the EPT BMG is more ductile than the as-cast BMG based on the observed shear band morphologies shown in Figs. 4 and 5.

Based on Yu et al.'s work [28], more secondary shear bands were observed after the annealing treatment of Zr-based BMGs. In this case, BMG becomes more brittle after annealing which is the opposite in comparison with the present EPT BMG. Using the free volume theory [36,37], the flow mechanism of BMGs can be interpreted in terms of the free volume, which can be treated as defects in amorphous alloys similar to vacancies in crystalline materials. Annealing would result in the structure relaxation of BMGs, such that the free volume is redistributed and annihilated which, in turn, results in the loss of plasticity.

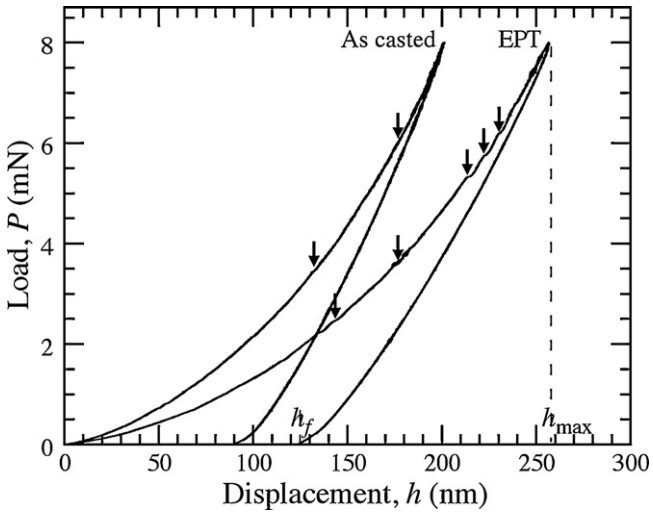

Fig. 2. Comparison of loading/unloading curves with the loading rate of 0.1 mN/s between as-cast and EPT BMGs. Observable serrations are marked by arrows.

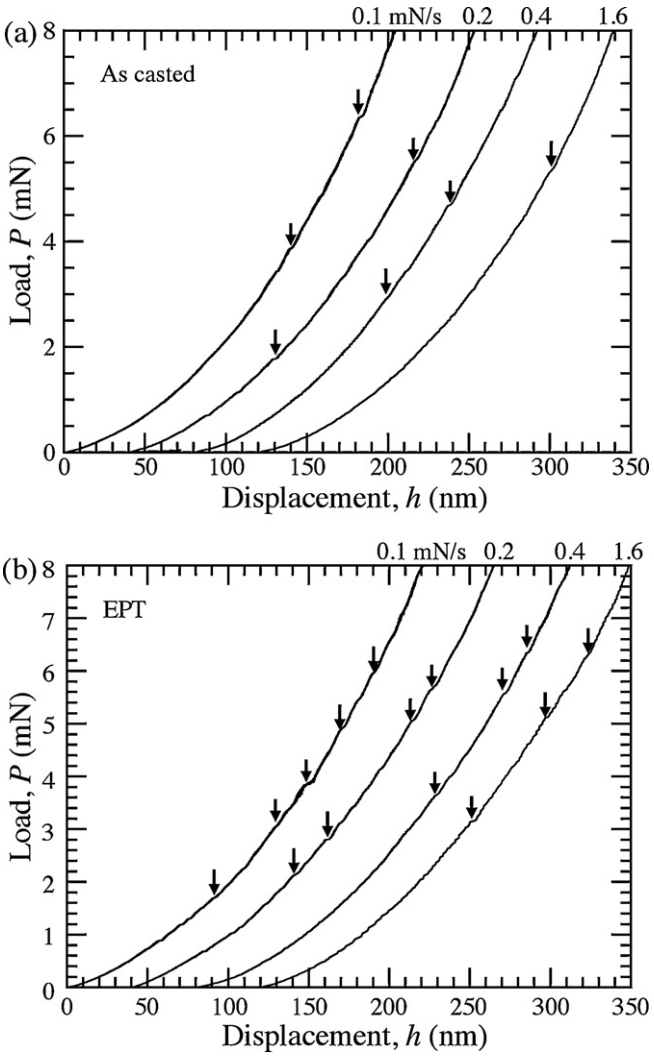

Fig. 3. Nanoindentation loading curves of (a) as-cast and (b) EPT BMGs showing more serrations for EPT-BMG for all loading rates.

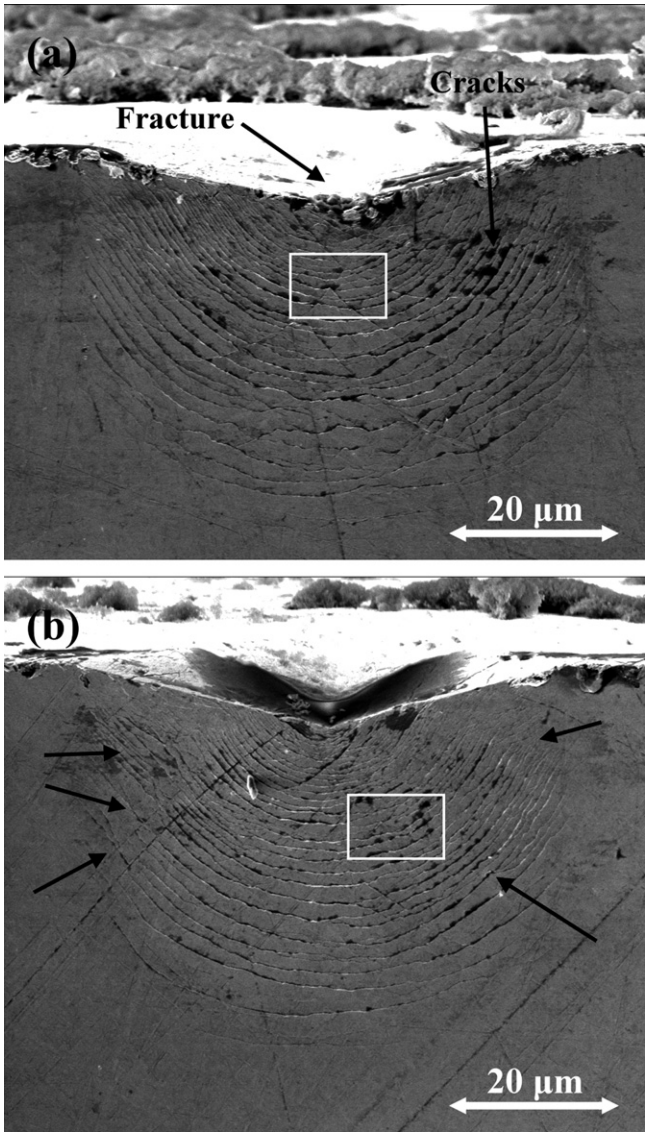

Fig. 4. Cross-sectional images of shear band patterns underneath a Vickers indentation for (a) as-cast and (b) EPT BMGs. Major features are: (i) a fractured region under indenter tip and severe cracking along semi-circular shear bands for as-cast BMG and (ii) less radial shear bands and more branching of semi-circular shear bands for EPT BMG. Regions marked with rectangles are enlarged and shown in Fig. 5(a) and (b).

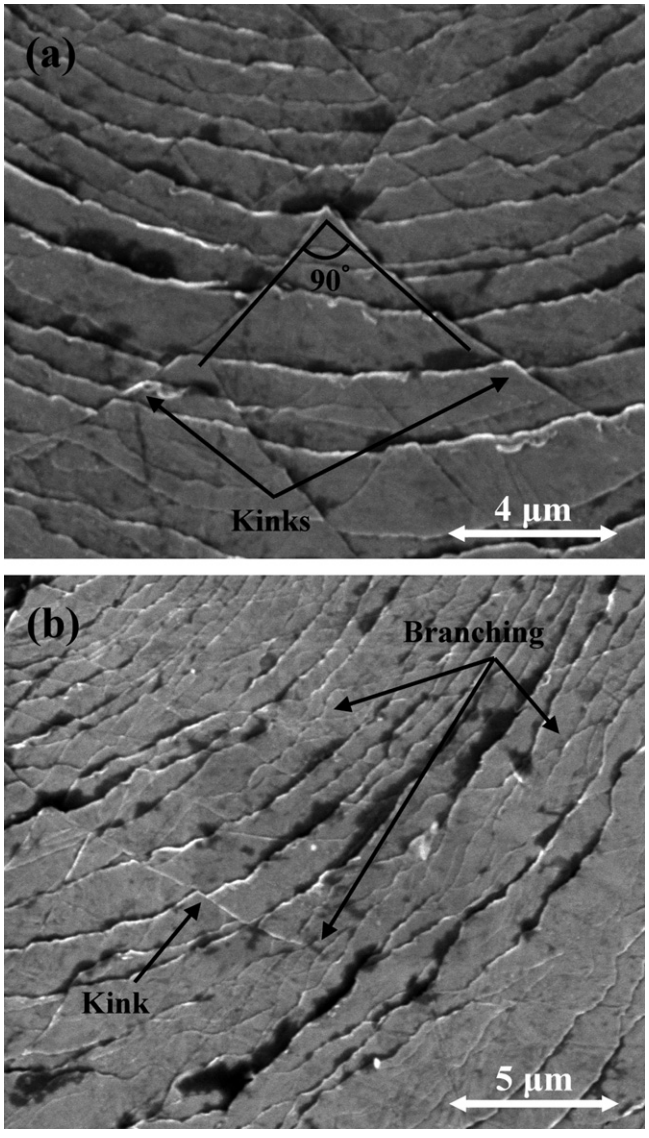

Fig. 5. Higher resolution images for (a) as-cast BMG showing more secondary shear bands and (b) EPT BMG showing more branching between semi-circular shear bands.

While the shear band morphology is correlated with the deformation mechanism, it can be concluded that EPT modifies the mechanical property of Zr-based BMG in a way different from annealing. Summarizing above observations, EPT lowers the shear band onset stress in Zr-based BMGs such that more shear bands can be initiated to provide plasticity, evidenced by both serrations in nanoindentation and the shear band morphology from the bond-interface method and Vickers indentation. For BMGs with limited macroscopic plasticity, the deformation is highly localized, such that the plastic strain is accumulated in a few very narrow shear bands exhibiting strain softening [37]. Plasticity enhancement can be achieved by dense pattern [38,39] or branching [40] of shear bands. It has been concluded that more homogeneous nucleation and continuous multiplication and branching of shear bands during deformation can better accommodate the applied strain and prevent damage from strain accumulation at localized shear bands [40]. Therefore, in our case plasticity is enhanced as branched shear bands delocalize deformation upon indentation. This also leads to less cracking between primary shear bands for the EPT-BMG as shown in Fig. 4b.

The above distinct results for the EPT-BMG might result from the different ways in heating up BMGs. For annealing, heating is achieved by heat conduction, convection, and radiation. However, for EPT, it is joule heating with electrons dissipating part of the electrical energy as heat, and the BMG is rapidly heated up from the internal. Also, part of the electrical energy could transfer the momentum to the atom by electron bombardment; i.e., the electromigration (EM) force. Studies in the nineties have found that DC would exert EM force on BMGs, inducing internal stress in the crystalline alloy. However, to result in the same magnitude of EM-force, the current density required in BMG is a few orders lower than that in the crystalline alloy (order of 10^3–10^4 versus 10^5–10^6 A/cm^2). This is because BMGs experience electron wind force in a more collective manner instead of individual atoms [41]. At a current density as low as 10^3 A/cm^2, EM effect was found to modify the magnetic and elastic properties and cause structural changes in BMGs [21,41,42]. Although the current density in the present work is much lower than 10^3 A/cm^2, difference should be

noted that EPT is cyclic and dynamic in terms of EM-force instead of being static in DC. It has been commented that both the stored elastic energy and free volume can promote the shear band formation [27]. Since EPT is an effective and rapid way to input energy into BMGs, it might store elastic energy, disturb the short-range order to create more free volume, and prevent annihilation of free volume in BMGs, such that the onset stress of shear band is lowered and there are more shear bands upon indentation loading. However, full understanding of the mechanism of EPT requires further studies

4. Conclusions

In conclusion, electropulsing treatment was applied on $(Zr_{53}Cu_{30}Ni_9Al_8)_{99.5}Si_{0.5}$ BMGs at 30 V/0.8 A with 15 Hz without resulting in crystallization. Bond-interface method revealed that the shear band morphology in the EPT BMG was different from that in the as-cast BMG. While there were more radial shear bands present in the as-cast BMG, more branching of the semi-circular shear bands was observed in the EPT BMG. Nanoindentation at different loading rates showed more serrations in the load–displacement curves for the EPT BMG than the as-cast BMG. This is in agreement with the observation of the shear band morphology that there is more branching of semi-circular shear bands after EPT. Although full understanding of the mechanism of EPT requires further studies, it can still be observed that EPT is a rapid treatment that can enhance plasticity of Zr-based BMGs by lowering the onset stress of shear bands and encourages branching of shear bands.

Acknowledgements

This project was supported by National Science Council, Taiwan under contract no. NSC100-2218-E-002-014. The authors would also like to acknowledge Dr. C.H. Shek of the City University of Hong Kong for his assistance on electropulsing equipment.

References

[1] W.L. Johnson, MRS Bull. 24 (1999) 42.
[2] A. Inoue, Acta Mater. 48 (2000) 279.
[3] C.H. Hsueh, H. Bei, C.T. Liu, P.F. Becher, E.P. George, Scr. Mater. 59 (2008) 111.
[4] H. Choi-Yim, R.D. Conner, F. Szuecs, Acta Mater. 50 (2002) 2737.
[5] Y.F. Sun, B.C. Wei, Y.R. Wang, J. Mater. Res. 20 (2005) 2386.
[6] R.D. Conner, R.B. Dandliker, W.L. Johnson, Acta Mater. 17 (1998) 6089.
[7] D.H. Bae, M.H. Lee, D.H. Kim, Appl. Phys. Lett. 83 (2003) 2312.
[8] H. Zhang, L.Z. Liu, Z.F. Zhang, J. Mater. Res. 21 (2006) 1375.
[9] D.V. Louzguine, H. Kato, A. Inoue, Appl. Phys. Lett. 84 (2004) 1088.
[10] M.L. Lee, Y. Li, C.A. Schuh, Acta Mater. 52 (2004) 4121.
[11] M. Chen, A. Inoue, W. Zhang, Phys. Rev. Lett. 96 (2006) 245502.
[12] S. Uchida, O. Shitaba, K. Oguri, J. Mater. Sci. 29 (1994) 5589.
[13] A.H. Bros, D.C. Dunand, MRS Bull. 23 (2007) 639.
[14] J.L. Zhang, H.B. Yu, J.X. Lu, Appl. Phys. Lett. 95 (2009) 071906.
[15] Z.W. Zhu, S.J. Zheng, H.F. Zhang, J. Mater. Res. 23 (2008) 941.
[16] W. Zhang, M.L. Sui, Y.Z. Zhou, Micron 34 (2003) 189.
[17] G.L. Hu, C.H. Shek, Y.H. Zhu, Mater. Trans. 51 (2010) 1390.
[18] Y.B. Jiang, G.Y. Tang, J. Mater. Res. 23 (2008) 2685.
[19] S. To, Y.H. Zhu, W.B. Lee, Mater. Trans. 50 (2009) 2772.
[20] Y.B. Jiang, G.Y. Tang, C.H. Shek, J. Mater. Res. 24 (2009) 1810.
[21] Z.H. Lai, H. Conrad, G.Q. Teng, Mater. Sci. Eng. A287 (2000) 238.
[22] T. Hao, H. Tanimoto, H. Mizubayashi, Mater. Trans. 46 (2005) 2898.
[23] Y.Z. Zhou, Q.S. Zhang, G.H. He, Mater. Lett. 57 (2003) 2208.
[24] J.L. Zhang, J.X. Lu, C.H. Shek, J. Phys.: Conf. Ser. 144 (2009) 012053.
[25] S. Nowak, P. Ochin, A. Pasko, J. Alloys Compd. 483 (2009) 139.
[26] C.A. Schuh, A.S. Argon, T.G. Nieh, J. Wadsworth, Philos. Mag. 83 (2003) 2585.
[27] C.A. Schuh, A.C. Lund, T.G. Nieh, Acta Mater. 52 (2004) 5879.
[28] G.S. Yu, J.G. Lin, M. Mo, Mater. Sci. Eng. A460–A461 (2007) 58.
[29] G.S. Yu, J.G. Lin, W. Li, J. Alloys Compd. 489 (2010) 558.
[30] H.W. Xie, Y.C. Li, D.K. Yang, J. Alloys Compd. 475 (2009) 501.
[31] U. Ramamurty, S. Jana, Y. Kawamura, K. Chattopadhyay, Acta Mater. 53 (2005) 705.
[32] S. Jana, U. Ramamurty, K. Chattopadhyay, Mater. Sci. Eng. A375–A377 (2004) 1191.
[33] S. Jana, R. Bhowmick, Y. Kawamura, Intermetallics 12 (2004) 1097.
[34] H. Zhang, X. Jing, G. Subhash, L.J. Kecskes, R.J. Dowding, Acta Mater. 53 (2005) 3849.
[35] S.Y. Kuan, X.H. Du, H.S. Chou, J.C. Huang, Surf. Coat. Technol. 206 (2011) 1116.
[36] D. Turnbull, M.H. Cohen, J. Chem. Phys. 52 (1970) 3038.
[37] F. Spaepen, Acta Metall. 25 (1977) 407.
[38] H. Bei, S. Xie, E.P. George, Phys. Rev. Lett. 96 (2006) 105503.
[39] Y. Zhang, W.H. Wang, A.L. Greer, Nat. Mater. 5 (2006) 857.
[40] J. Das, M.B. Tang, K.B. Kim, R. Theissmann, F. Baier, W.H. Wang, J. Eckert, Phys. Rev. Lett. 94 (2005) 205501.
[41] R. Takemoto, M. Nagatas, Acta Mater. 44 (1996) 2787.
[42] R. Takemoto, H. Mizubayashi, Acta Metall. Mater. 43 (1995) 1495.